

Path Integral Methods

Nancy Makri

School of Chemical Sciences, University of Illinois, Urbana, Illinois 61801

Abbreviations

FPF = filtered propagator functional; MCPI = Monte Carlo path integral; MEM = maximum entropy method; QUAPI = quasi-adiabatic propagator path integral

1 INTRODUCTION

The path integral approach was introduced by Feynman¹ in a seminal paper published in 1948. It provides an alternative formulation of time-dependent quantum mechanics, equivalent to that of Schrödinger. Since its inception, the path integral has found innumerable applications in many areas of physics and chemistry. Its main attractions can be summarized as follows: the path integral formulation offers an ideal way of obtaining the classical limit of quantum mechanics; it provides a unified description of quantum dynamics and equilibrium quantum statistical mechanics; it avoids the use of wavefunctions and thus is often the only viable approach to many-body problems; and it leads to powerful influence functional methods for studying the dynamics of a low-dimensional system coupled to a harmonic bath.

The path integral formulation builds on the principle of superposition, which leads to the celebrated quantum interference observed in the microscopic world. Thus, the amplitude for making a transition between two states is given by the sum of amplitudes along all possible paths connecting these states in the specified time, a concept familiar from wave optics. Classical behavior is recovered through phase cancellation among paths whose phase is not stationary.

The present article presents an introduction to the path integral formulation of quantum dynamics and quantum statistical mechanics along with numerical procedures useful in these areas and in electronic structure theory. Section 2 describes the path integral formulation of the quantum mechanical propagator and its relation to the more conventional Schrödinger description. That section also derives the classical limit and discusses the connection with equilibrium properties in the canonical ensemble. Numerical techniques are described in section 3. Selective chemical applications of the path integral approach are presented in section 4 and section 5 concludes.

2 THE PATH INTEGRAL

For a particle of mass m in one dimension, the amplitude to get from a point x_a at the time t_a to the point x_b at the time t_b is expressed in the path integral formulation as a sum of contributions from all conceivable paths that connect these points². The contribution of each path $x(t)$ is proportional to a phase that is given by the action functional $S[x(t)]$ along that path in units of Planck's constant \hbar :

$$K(x_b, t_b; x_a, t_a) \propto \sum_{\substack{\text{all paths } x(t) \\ \text{with } x(t_a)=x_a, x(t_b)=x_b}} e^{iS[x(t)]/\hbar}$$

Classical and non-classical paths enter this expression with the same weight. In the classical limit $\hbar \rightarrow 0$ small variations of a path generally result in large changes in the phase S/\hbar . Because of destructive phase interference, the contributions of most paths sum to zero in this limit. Constructive interference results from paths whose action is stationary. Assuming a simple Lagrangian of the form $L(x, \dot{x}) = \frac{1}{2}m\dot{x}^2 - V(x)$ and using a stationary phase path $x_{\text{SP}}(t)$ as the reference in terms of which the action of a nearby path $x_{\text{SP}}(t) + \delta x(t)$ with the same endpoints is expanded, one obtains

$$0 = \delta S \equiv S[x_{\text{SP}}(t) + \delta x(t)] - S[x_{\text{SP}}(t)]$$

$$= \int_{t_a}^{t_b} \left\{ \frac{1}{2} m (\dot{x}_{\text{SP}}(t) + \delta \dot{x}(t))^2 - V(x_{\text{SP}}(t) + \delta x(t)) \right\} dt - \int_{t_a}^{t_b} \left\{ \frac{1}{2} m \dot{x}_{\text{SP}}(t)^2 - V(x_{\text{SP}}(t)) \right\} dt$$

Equation 1

Expansion of the potential in a Taylor series through first order in the path variation gives

$$\delta S \approx \int_{t_a}^{t_b} m \dot{x}_{\text{SP}}(t) \delta \dot{x}(t) dt - \int_{t_a}^{t_b} V'(x_{\text{SP}}(t)) \delta x(t) dt.$$

Equation 2

Upon integrating by parts the first term and using the boundary conditions $\delta x(t_a) = \delta x(t_b) = 0$, the last equation leads to the result

$$m \ddot{x}_{\text{SP}}(t) + V'(x_{\text{SP}}(t)) = 0$$

Equation 3

which shows that in the classical limit only paths satisfying Newton's law contribute to the amplitude.

Using Eq. (1) and the superposition principle for the evolution of a wavefunction,

$$\Psi(x; t + \delta t) = \int K(x, t + \delta t; x_0, t) \Psi(x_0; t) dx_0$$

Equation 4

one can recover the time-dependent Schrödinger equation.²

Conversely, one can derive the path integral from the Schrödinger formulation of quantum mechanics. The amplitude given in Eq. (1) is the quantum mechanical propagator, i.e. the coordinate representation of the Green function for the time-dependent Schrödinger equation. For a time-independent Hamiltonian $H \equiv T + V$, where T and V are the kinetic and potential energy operators, respectively,

$$K(x_b, t_b; x_a, t_a) \equiv \langle x_b | \exp\left(-\frac{i}{\hbar} H(t_b - t_a)\right) | x_a \rangle = \langle x_b | \left(\exp\left(-\frac{i}{\hbar} H \Delta t\right) \right)^N | x_a \rangle$$

Equation 5

where $\Delta t \equiv (t_b - t_a)/N$ and N is an integer. Inserting complete sets of position states, one obtains the identity

$$K(x_b, t_b; x_a, t_a) = \int_{-\infty}^{\infty} dx_1 \cdots \int_{-\infty}^{\infty} dx_{N-1} \prod_{k=1}^N \langle x_k | \exp(-iH\Delta t/\hbar) | x_{k-1} \rangle$$

Equation 6

where $x_0 \equiv x_a$ and $x_N \equiv x_b$. By choosing an appropriate value of N the time step Δt can be made sufficiently small such that the short time propagators in the last equation can be approximated using the Trotter product rule

$$\exp\left(-\frac{i}{\hbar} H \Delta t\right) \approx \exp\left(-\frac{i}{\hbar} V \frac{\Delta t}{2}\right) \exp\left(-\frac{i}{\hbar} T \Delta t\right) \exp\left(-\frac{i}{\hbar} V \frac{\Delta t}{2}\right)$$

Equation 7

leading to the result

$$\langle x_k | \exp\left(-\frac{i}{\hbar} H \Delta t\right) | x_{k-1} \rangle \approx \left(\frac{m}{2\pi i \hbar \Delta t}\right)^{1/2} \exp\left(\frac{i}{\hbar} \frac{m}{2\Delta t} (x_k - x_{k-1})^2 - \frac{i}{\hbar} \frac{\Delta t}{2} (V(x_k) + V(x_{k-1}))\right)$$

Equation 8

Use of this result in Eq. (6) leads to the following discretized path integral expression for the propagator:

$$K(x_b, t_b; x_a, t_a) \approx \left(\frac{mN}{2\pi i \hbar (t_b - t_a)}\right)^{N/2} \int_{-\infty}^{\infty} dx_1 \cdots \int_{-\infty}^{\infty} dx_{N-1} \times \exp\left(\frac{i}{\hbar} \frac{mN}{2(t_b - t_a)} \sum_{k=1}^N (x_k - x_{k-1})^2 - \frac{i}{\hbar} \frac{t_b - t_a}{2N} [V(x_k) + V(x_{k-1})]\right)$$

Equation 9

which becomes an equality in the limit $N \rightarrow \infty$. With finite values of the time step the Feynman paths in Eq. (9) are discretized (see Figure 1). The exponent in the last expression is easily recognized as the trapezoid rule discretization of the action in Feynman's *ansatz*, Equation (1). Another alternative to the slicing employed above involves expansion of the paths in Fourier series.³

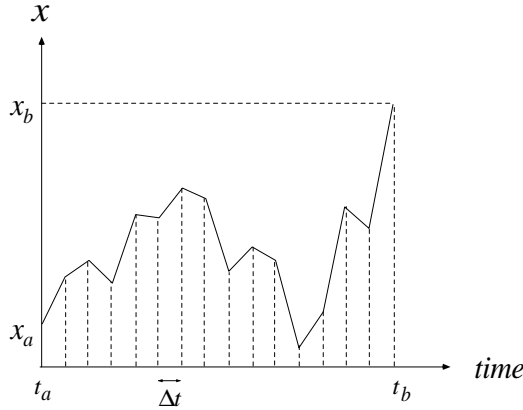


Fig. 1. A discretized path that connects the points (x_a, t_a) and (x_b, t_b) .

Because the quantum mechanical time evolution operator $\exp(-iH(t_b - t_a)/\hbar)$ has the same mathematical form with the Boltzmann operator $\rho \equiv \exp(-\beta H)$, where $\beta = 1/k_B T$ is the inverse temperature in units of the Boltzmann constant k_B , the above path integral formalism can be straightforwardly generalized to yield equilibrium properties in the canonical ensemble.⁴ Making the formal identification $t_b - t_a \equiv -i\hbar\beta$, the canonical density matrix is given by the following “imaginary time” path integral expression:

$$\rho(x_b, x_a) \equiv \langle x_b | \exp(-\beta H) | x_a \rangle = \lim_{N \rightarrow \infty} \left(\frac{mN}{2\pi\hbar^2 \beta} \right)^{N/2} \int_{-\infty}^{\infty} dx_1 \cdots \int_{-\infty}^{\infty} dx_{N-1} \\ \times \exp \left(-\frac{mN}{2\hbar^2 \beta} \sum_{k=1}^N (x_k - x_{k-1})^2 - \frac{\beta}{2N} [V(x_k) + V(x_{k-1})] \right)$$

Equation 10

Although identical in structure to Eq. (9) for the real time propagator, the path integral representation of the canonical density matrix involves a real-valued integrand in which different paths enter with different weights. These features are extremely useful in numerical calculations (see section 3).

When the canonical partition function or equilibrium averages of local operators are considered, the trace operation constrains all paths to be closed. For this reason, a single quantum particle becomes isomorphic⁵ to a polymer necklace of N fictitious classical particles which are connected with harmonic springs of force constant $mN/\hbar^2 \beta^2$ and each of them experiences a potential equal to $V(x)/N$. In the classical limit this necklace collapses to a single point.

All the above expressions are straightforward to generalize formally to spinless systems of many coupled degrees of freedom. The path integral representation of the quantum mechanical propagator is particularly useful for eliminating harmonic degrees of freedom. Because the latter enter the path integral, Eq. (9), as Gaussian functions they can be integrated out analytically⁶, leading to reduced dimension descriptions that form the basis of powerful analytic and numerical treatments (see, for example, references 2, 4, 7, 8 and the next section).

Within the path integral formulation, identical particles are dealt with by adding (or subtracting) the appropriate amplitudes corresponding to particle permutations in a way similar to that employed in the symmetrization (or antisymmetrization) of wavefunctions. This procedure introduces negative amplitudes in finite temperature calculations of many-fermion systems, leading to significant numerical difficulties which are addressed in the next section.

3 NUMERICAL METHODS

3.1 Equilibrium properties

The discretized path integral expression of the canonical density matrix leads to extremely useful numerical algorithms for evaluating finite temperature properties of many-particle spinless or boson systems not treatable by other techniques. The required multidimensional integrals are evaluated by Monte Carlo methods, which have been reviewed extensively elsewhere. Here we outline the general features of such calculations using as an example the Boltzmann average of a quantum mechanical operator A , which takes the form

$$\langle A \rangle \equiv \frac{\text{Tr} \left(e^{-\beta H} A \right)}{\text{Tr} e^{-\beta H}} = Q_\beta^{-1} \int d^n \mathbf{x} \langle \mathbf{x} | e^{-\beta H} A | \mathbf{x} \rangle$$

Equation 11

where $\mathbf{x} \equiv (x_1, \dots, x_n)$ is the vector of n Cartesian coordinates of all the particles and Q_β is the canonical partition function. If A is diagonal in the coordinate representation, its expectation value becomes

$$\langle A \rangle = \lim_{N \rightarrow \infty} \int dx_{1,1} \cdots dx_{1,N} \cdots dx_{n,1} \cdots dx_{n,N} \sigma(x_{1,1}, \dots, x_{1,N}, \dots, x_{n,1}, \dots, x_{n,N}) A(x_{1,N}, \dots, x_{n,N}),$$

Equation 12

where

$$\begin{aligned} & \sigma(x_{1,1}, \dots, x_{1,N}, \dots, x_{n,1}, \dots, x_{n,N}) \\ &= Q_{\beta}^{-1} \exp\left(-\sum_{j=1}^n \frac{m_j N}{2\hbar^2 \beta} \sum_{k=1}^N (x_{j,k} - x_{j,k-1})^2 - \frac{\beta}{N} \sum_{k=1}^N V(x_{1,k}, \dots, x_{n,k})\right) \end{aligned}$$

Equation 13

Here $x_{j,k}$ denotes the k^{th} discretization of coordinate x_j and $x_{j,0} = x_{j,N}$. In practice, Eq. (12) is evaluated with N sufficiently large for the error introduced through the Trotter factorization of the short time propagators to be within the acceptable tolerance.

The $n \times N$ dimensional integral in Eq. (12) is usually performed with Monte Carlo methods⁹ using σ as the normalized sampling function. Note that in order to achieve rapid convergence it is often necessary to perform collective coordinate moves in the Monte Carlo random walk. For a comprehensive description of the Monte Carlo path integral (MCPI) method along with various advanced numerical procedures employed in equilibrium path integral calculations the reader is referred to reference 10 and to *Monte Carlo Simulation Methods for Polymers*.

The path integral representation of quantum statistical mechanics also leads to powerful mixed quantum-classical simulation schemes. By virtue of the classical polymer isomorphism discussed in the previous section, the quantum partition function of a particle is formally equivalent to the classical partition function for a polymer ring of classical pseudo-particles. Equilibrium properties for a quantum particle in a classical solvent can be calculated by “immersing” the polymer in the classical solvent and treating the combined many-particle system by standard Monte Carlo (see also *Monte Carlo Methods for Studying Polymers and Complex Fluids*) or molecular dynamics techniques; the latter often provide a viable alternative to importance sampling methods.

Severe problems arise when two or more identical fermions are treated explicitly. As configurations corresponding to identical particle exchange enter with the same weight but alternating signs, the integrand is no longer positive definite and the Monte Carlo procedure must be modified. Although positive sampling functions can still be identified, the frequent sign change causes dramatic cancellation and eventually renders Monte Carlo methods unstable. This behavior, known as the “sign problem”, continues to plague quantum Monte Carlo simulations of many-electron systems such that converged results can be extracted only in a few special cases or by introducing approximations that alleviate the phase cancellation.¹¹

3.2 Dynamical properties

Unlike finite temperature equilibrium properties of spinless or boson systems, which can be evaluated efficiently by Monte Carlo path integral methods, dynamical quantities present a considerable challenge. As all paths enter the primitive discretized path integral, Equation (3), with the same weight, one needs to sample the entire volume of integration and importance sampling does not offer an advantage. Most importantly, the rapid phase oscillation of the integrand results in enormous cancellation which cannot be dealt with by Monte Carlo procedures. This behavior is yet another manifestation of the sign problem and hinders dynamical path integral calculations, regardless of the particles’ spin.¹²

The situation can be improved by constructing improved propagators which employ appropriate projection operators¹³ or physically motivated reference systems¹⁴ in the discretization of the path integral. These schemes lead to path integral expressions where the integrand is relatively localized and only mildly oscillatory with respect to each path integral vari-

able. However, the effect of the residual oscillations (which are essential for reproducing quantum interference effects) is amplified in multidimensional space, leading to dramatic cancellation which renders Monte Carlo schemes inadequate for calculating the dynamics beyond a few time steps. Another possibility, also successful at short time, is to bias the sampling near classical paths, where the phase is stationary and therefore phase cancellation is minimal.¹⁵ This approach also suffers from the sign problem at longer times, as many stationary phase paths begin to contribute with different phases that generally interfere destructively. For reviews of these approaches the reader is referred to references 13 and 16.

Another possibility for extracting dynamical properties is via analytic continuation of imaginary time quantities,^{12,17,18} which are relatively straightforward to calculate. Analytic continuation methods are successful only if accurate data points are available. As a consequence, the presence of statistical error in the imaginary time data renders the process of analytic continuation to real time unstable in general.

Recently, maximum entropy image enhancement techniques¹⁹ have been successfully applied to a variety of ill-conditioned problems, including the inversion of imaginary time quantities to obtain spectral properties. The presence of noise in equilibrium MCPI naturally limits the spectral information contained in these data. The maximum entropy method²⁰ (MEM) finds the spectrum that corresponds to the largest number of ways of reproducing the data. By construction, the resulting spectrum has maximum entropy (in the information theory definition) subject to a number of constraints.²¹ Recent applications²² indicate that the maximum entropy method can yield semi-quantitative estimates of absorption spectra in solution and the corresponding real-time correlation functions up to moderate times. As such, it will find a variety of uses in condensed phase dynamics and spectroscopy as long as long-time information or low-frequency features of a spectrum are not required.

To this date, no stable simulation methods are known which are successful at obtaining quantum dynamical properties of arbitrary many-particle systems over long times. However, significant progress has been made recently in the special case where a low-dimensional nonlinear system is coupled to a dissipative bath of harmonic oscillators. The system-bath model can often provide a realistic description of the effects of common condensed phase environments on the observable dynamics of the microscopic system of interest. A typical example is that of an impurity in a crystalline solid, where the harmonic bath arises naturally from the small-amplitude lattice vibrations. The harmonic picture is often relevant even in situations where the motion of individual solvent atoms is very anharmonic; in such cases validity of the linear response approximation can lead to Gaussian behavior of appropriate *effective* modes by virtue of the central limit theorem.^{2,23,24}

The remaining of this subsection focuses on the following system-bath Hamiltonian:

$$H = \frac{p_s^2}{2m_0} + V_0(s) + \sum_j \left(\frac{p_j^2}{2m_j} + \frac{1}{2} m_j \omega_j^2 x_j^2 - c_j s x_j \right)$$

Equation 14

Here s denotes the coordinate(s) of the quantum particle and x_j are the coordinates of the harmonic oscillator modes which are linearly coupled to the system and which constitute the bath. For simplicity the coupling functions are assumed linear in the system coordinate as well, although extension of the procedure that follows to a more general coupling form of the type $f_j(s)x_j$ is straightforward.

Accurate propagators for the Hamiltonian of Equation (14) are constructed by including the potential along the one-dimensional adiabatic path defined by the relations $x_j = c_j s / m_j \omega_j^2$ to construct a reference Hamiltonian

$$H_0 = \frac{p_s^2}{2m_0} + V_0(s) - \sum_j \frac{c_j^2 s^2}{2m_j \omega_j^2}.$$

Equation 15

The reference propagator is calculated numerically in terms of the M lowest energy eigenfunctions Φ_k and eigenvalues E_k of H_0 :

$$\langle s_b | e^{-iH_0\Delta t/\hbar} | s_a \rangle = \sum_{k=1}^M \Phi_k(s_b) \Phi_k(s_a) e^{-iE_k\Delta t/\hbar}$$

Equation 16

The remaining terms in the system-bath Hamiltonian correspond to linearly displaced harmonic oscillators which enter the path integral in a Gaussian fashion. Following the procedure of Feynman and Vernon,⁶ these Gaussian variables are integrated out, leading to an influence functional which accounts for nonadiabatic corrections to the exact dynamics along the adiabatic path included in the reference propagator. The resulting quasi-adiabatic propagator path integral (QUAPI) expressions¹⁴ converge with relatively large time steps.

Quantum mechanical observables for the system of interest can be obtained from the reduced density matrix,

$$\tilde{\rho}(s'', s'; t) \equiv Z^{-1} \text{Tr}_b \langle s'' | e^{-iHt/\hbar} \rho(0) e^{iHt/\hbar} | s' \rangle$$

Equation 17

(where Z is the canonical partition function), whose QUAPI representation reads, assuming that system and bath are not correlated at $t = 0$:

$$\begin{aligned} \tilde{\rho}(s'', s'; t) &= \int ds_0^+ \int ds_1^+ \cdots \int ds_{N-1}^+ \int ds_0^- \int ds_1^- \cdots \int ds_{N-1}^- \langle s'' | e^{-iH_0\Delta t/\hbar} | s_{N-1}^+ \rangle \cdots \langle s_1^+ | e^{-iH_0\Delta t/\hbar} | s_0^+ \rangle \\ &\quad \times \langle s_0^+ | \tilde{\rho}(0) | s_0^- \rangle \langle s_0^- | e^{iH_0\Delta t/\hbar} | s_1^- \rangle \cdots \langle s_{N-1}^- | e^{iH_0\Delta t/\hbar} | s' \rangle \\ &\quad \times F(s_0^+, s_1^+, \dots, s_{N-1}^+, s'', s_0^-, s_1^-, \dots, s_{N-1}^-, s'; \Delta t) \end{aligned}$$

Equation 18

Here $\{s_0^+, s_1^+, \dots\}$ and $\{s_0^-, s_1^-, \dots\}$ denote discretizations of the forward and backward path employed in the path integral representation of the forward and reverse time evolution operators, respectively. The influence functional has the structure

$$F = \exp \left(-\frac{1}{\hbar} \sum_{k=0}^N \sum_{k'=1}^k (s_k^+ - s_k^-) (\eta_{kk'} s_{k'}^+ - \eta_{kk'}^* s_{k'}^-) \right)$$

Equation 19

where the coefficients $\eta_{kk'}$ are discretized versions of the bath force autocorrelation function, which depends on the spectral features of the harmonic medium as well as the system-bath coupling coefficients.

In the absence of coupling to a bath the influence functional is equal to unity. In that limit the path integral variables are coupled only to their nearest neighbors in time, i.e., s_k is coupled only to $s_{k\pm 1}$. This fact is a consequence of the Markovian nature of the dynamics for the quantum particle alone, as the wavefunction for the latter obeys the first-order Schrödinger differential equation. Because of this structure, the path integral in the absence

of influence functional interactions can be broken into a sequence of one-dimensional integrations which form the basis of iterative matrix multiplication schemes and their variants that are routinely used for wavefunction propagation of small molecules²⁵ (see also *Time Dependent Quantum Methods*).

The wavefunction for the system-bath Hamiltonian in full dimensionality also satisfies the time-dependent Schrödinger equation. However, the Markovian character of the dynamics is lost when the bath is integrated out to produce path integral expressions in reduced dimension space (see Figure 2). Indeed, the influence functional contains interactions between variables that may be separated by many time steps. This structure is reminiscent of the memory friction kernel in the classical generalized Langevin equation.²⁶ As multidimensional integration methods are not successful in real time, evaluation of the reduced density matrix is problematic at intermediate to long times. The current status of MCPI methods applied to system-bath models is described in Ref. 27 and in *Computation of phase diagrams for electronic systems*.

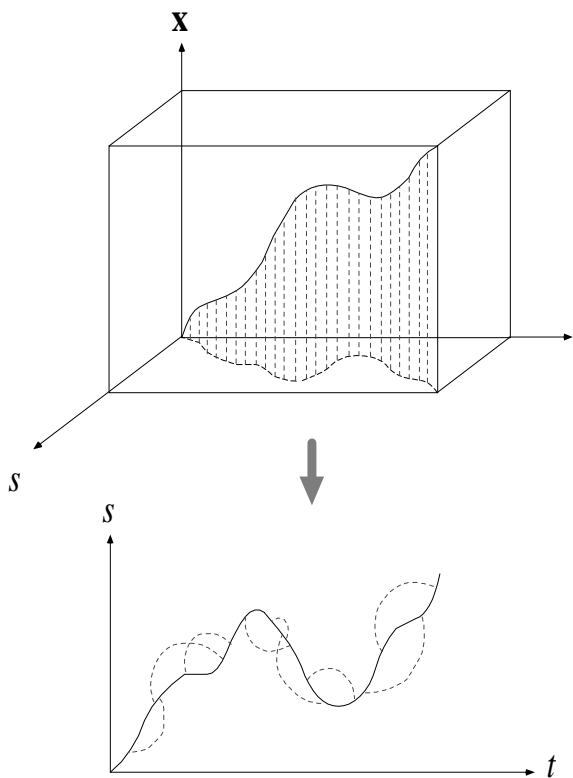


Fig. 2. Schematic representation of a Feynman path in full-dimension system-bath space and its projection onto the reduced-dimension space characterized by the system coordinate alone. The gray curved lines indicate some of the nonlocal influence functional interactions arising from this projection.

Fortunately, progress can be made in cases where the bath corresponds to a condensed medium. Because condensed phase correlation functions decay within a finite interval, the effective length of nonlocal influence functional interactions is finite. Dropping negligible long-range correlations allows decomposition of the multidimensional path integral into a sequence of lower-dimensional operations (see Figure 3). Specifically, a reduced density functional (a multi-time object) of path segments that carry statistically significant weight can be propagated forward in time via multiplication with an appropriate propagator functional.²⁸ In discrete time language the reduced density functional becomes a vector and the propagator a matrix, such that the scheme reduces to matrix-vector multiplication, the essential difference from wavefunction propagation schemes being that the present case requires

the use of larger matrices. The filtered propagator functional (FPF) allows iterative evaluation of the real-time path integral over long time intervals; for this reason it enables *ab initio* simulations of quantum dissipative systems not feasible by other means.

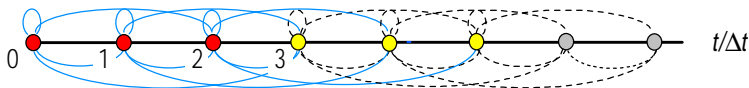


Fig. 3. Diagrammatic representation of the path integral interactions in a case where the memory length is equal to three time steps. The reduced density functionals that start at $t = 0$ and $t = 3\Delta t$ consist of paths specified by the time points shown as red and yellow circles, respectively. The coupling terms in the propagator connecting these two reduced density functionals are shown as cyan lines.

4 ILLUSTRATIVE EXAMPLES

In this section we discuss a few representative applications of numerical path integral methods. The presentation that follows is not intended to replace detailed reviews of path integral simulations. The calculations discussed below serve as illustrative examples of the range of chemical questions that can be successfully addressed with path integral methods. For more information and for discussion of numerous other important applications of the path integral in chemistry and physics the reader is referred to comprehensive review articles and recent books.

4.1 Structure and spectroscopy of excess electrons in classical liquids and clusters

Path integral methods have proven very useful for studying the equilibrium properties of excess electrons in clusters and classical fluids, and recently spectral properties have begun to be accessible as well. Such studies have revealed a wealth of information about the nature of these electronic states and the corresponding solvent structure. Numerous reviews on this subject have appeared in the last decade.

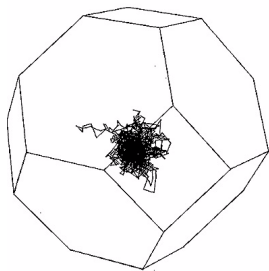


Fig. 4. Electron path of a representative configuration in an octahedral unit simulation cell containing 300 water molecules (not drawn). The beads of the cyclic polymer are connected by straight lines. Adapted from Ref. 29.

The equilibrium properties of an excess electron in molten alkali halide solvent and in liquid water have been probed via imaginary time path integral simulations using pseudopotentials to model the electron-solvent interaction.^{29,30} By employing the classical isomorphism, the electron was mapped onto a classical polymer interacting with solvent molecules and various properties of the combined system were probed via molecular dynamics techniques. These simulations confirmed the conventional picture, in which the electron occupies a cavity surrounded by solvation shells similar to those observed around negative ions. A typical configuration of the electron necklace, forming a cavity in water, is shown in Figure 4.

Unlike ion-filled cavities, however, large quantum fluctuations of the electronic density tend to suppress patterns in the radial electron-water correlation function.

By contrast, excess electrons in non-polar solvents can exhibit delocalized behavior as well. MCPI simulations have revealed cavity formation in a helium environment and delocalized behavior in the more polarizable xenon.³¹ Similar patterns were observed in alkane solvents. While the electron always exists in an extended state in a methane solvent, a transition to a self-trapping state was found in the case of ethane at a critical value of the fluid density.³²

Recently the MEM was applied to the calculation of optical absorption spectra and correlation functions for an excess electron in water and supercritical noble gas fluids.²² Semi-quantitative agreement with experimental spectra was found in the case of water, where the electron is confined in cavities. In addition, the electron mobility was successfully modeled in the supercritical helium environment where the electronic states are extended.

Excess electrons in clusters also exhibit the above structural characteristics as well as other quantum mechanical effects that arise when the electron wavelength is comparable to the cluster diameter. Path integral studies of an excess electron in alkali halide clusters³³ have established the existence of internal cavity structures and of extended surface states. Dissociative attachment, leading to the formation of an isolated alkali atom, and structural isomerization have also been observed. Similar calculations have demonstrated the prevalence of surface states in water clusters.³⁴ Representative structures are shown in Figure 5.

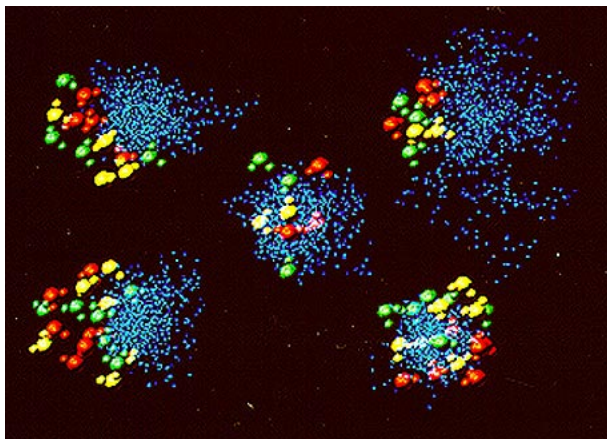


Fig. 5. Cluster configurations of $(\text{H}_2\text{O})_n^-$ via quantum path integral molecular dynamics simulations. Colored balls, large and small, correspond to oxygen and hydrogen, respectively. Colors of balls are chosen for visual perspective. The blue dots represent the electron (bead) distributions. Shown at the center is $(\text{H}_2\text{O})_8^-$ for a static molecular configuration. From top right and going counterclockwise: (i) diffuse surface state of $(\text{H}_2\text{O})_8^-$; (ii) surface state of $(\text{H}_2\text{O})_{12}^-$; (iii) surface state of $(\text{H}_2\text{O})_{18}^-$ (most stable structure); (iv) internal state of $(\text{H}_2\text{O})_{18}^-$. Adapted from Ref. 34.

4.2 Electronic structure of ground states

Knowledge of the partition function at low temperature can be used to obtain the ground state energy E_0 of a system, i.e.,

$$E_0 = -\lim_{\beta \rightarrow \infty} \left(\frac{1}{\beta} \int d^n \mathbf{x} \langle \mathbf{x} | e^{-\beta H} | \mathbf{x} \rangle \right).$$

Equation 20

The last equation is known as the Feynman-Kac formula and provides the starting point for quantum Monte Carlo electronic structure calculations. The reader is referred to references 11, 35 and 36 and to *Quantum Monte Carlo Methods for Electronic Structure* for recent reviews of such methods.

4.3 Tunneling splittings

Generally, the Feynman-Kac approach is not useful for obtaining properties of excited states. Some progress can be made by imposing appropriate orthogonality constraints; however, because the nodes of excited state wavefunctions are not known with precision *a priori*, such calculations require a certain degree of skill.

A different situation arises in the specific case of a symmetric double minimum potential, where the two lowest energy states are separated by a small tunneling splitting. Because this splitting is small compared to the energy gap from the next excited state, an appropriate temperature range can be found where both members of the tunneling doublet are populated while the contribution of higher excitations is negligible. Furthermore, taking into account the symmetric/antisymmetric nature of the ground and first excited state wavefunctions, one can show³⁷ that the tunneling splitting is simply related to the ratio of diagonal and off-diagonal elements of the equilibrium density matrix with respect to two symmetrically located coordinate points. Employing equilibrium path integral methods to calculate the density matrix elements yields the ground state tunneling splitting. This method is stable and accurate even when the tunneling frequency is very small.

This approach has been applied to the calculation of frequencies for two-, three-, four-, and six-particle exchange in crystal ^3He .³⁷ These calculations revealed that pair exchange is most frequent, followed closely by planar four-atom exchange and triplet exchange. In addition, that work concluded that the largest exchange frequencies scale with density as the 20th power, in good agreement with experiment.

The above treatment has also been generalized to utilize non-symmetrically related configurations.³⁸ Application gave the tunneling splitting as a function of interionic distance in aqueous $\text{Fe}^{2+} - \text{Fe}^{3+}$ electron transfer and probed the nature of the quantum instanton-type paths connecting the two ions.³⁹ An electron path corresponding to the transition state of the reaction is depicted in Figure 6. The centroid of the electron path lies midway between the two ions.

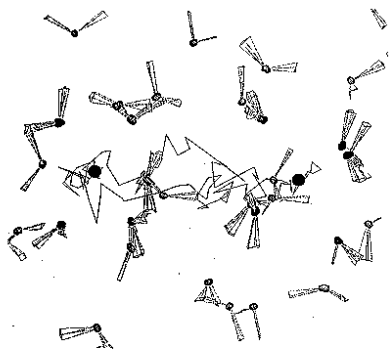


Fig. 6. A transition state from the simulated aqueous $\text{Fe}^{2+} - \text{Fe}^{3+}$ electron transfer. The two larger dark circles are the irons 5.5 Å apart and the jagged lines connecting them is one path of the resonating electron. The Feynman paths of the quantized water molecules show the librations. Only a few of the hundreds of the simulated waters are depicted. Adapted from Ref. 39.

4.4 Canonical reaction rates in the condensed phase

Barrier crossing phenomena are fundamental in chemistry. In many situations barrier crossing events correspond to first-order kinetics characterized by a rate constant. Because the dynamics of such processes corresponds to infrequent events, direct simulation of a reaction from reactants to products can be extremely inefficient. A much better approach is offered by the reactive flux formalism⁴⁰ which expresses the reaction rate in terms of the flux crossing a fictitious dividing surface that separates reactants from products. Even though the reactive flux method offers a numerically advantageous approach compared to direct simulation of the reaction itself, fully quantum mechanical evaluation of the flux correlation function in polyatomic systems remains computationally intractable. Nevertheless, this formalism is closely connected to and has served as the starting point for a variety of semiclassical or quantum mechanical transition state approximations for adiabatic and nonadiabatic reactions⁴¹⁻⁴⁵ which can be evaluated by means of equilibrium path integral calculations (see also *Chemical Reaction Rates and Simulation and Theory of Barrier Crossings*). Numerous reactive processes have been probed via Monte Carlo or molecular dynamics path integral calculations in imaginary time. Illustrative examples include the rates for electron exchange in the aqueous $\text{Co}(\text{NH}_3)_6^{2+} / \text{Co}(\text{NH}_3)_6^{3+}$ and $\text{Fe}^{2+} / \text{Fe}^{3+}$ pairs^{46,47} and diffusion of hydrogen in metals⁴⁸ or on metal surfaces.⁴⁹

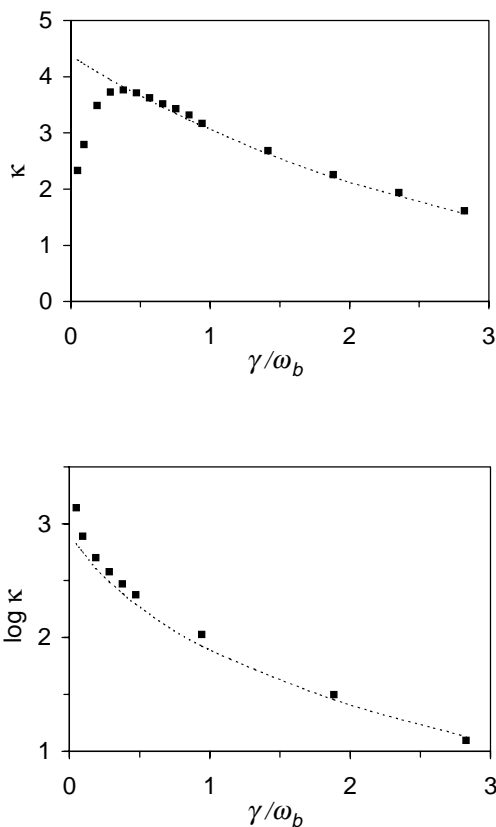


Fig. 7. Quantum transmission coefficient for a symmetric double well potential interacting with a generic dissipative medium as a function of friction strength γ . The barrier height is denoted E_b and ω_b is the imaginary frequency at the top of the potential barrier. Solid squares: QUAPI results. Dashed line: results of centroid-density quantum transition state theory. (a) $E_b/k_bT = 10$ (activated regime with tunneling contributions). (b) $E_b/k_bT = 30$; for the first six data points (at small friction) the temperature is below crossover. Data from Ref. 51.

Recently, a QUAPI procedure was developed⁵⁰ suitable for evaluating the full flux correlation function⁵¹ in the case of a one-dimensional quantum system coupled to a dissipative harmonic bath and applied to obtain accurate quantum mechanical reaction rates for a symmetric double well potential coupled to a generic environment.⁵² These calculations confirmed the ability of analytical approximations to provide a nearly quantitative picture of such processes in the activated regime, where the reaction rate displays a Kramers turnover as a

function of solvent friction and quantum corrections are small or moderate.⁵³ They also emphasized the significance of dynamical effects not captured in quantum transition state models, in particular under small dissipation conditions where imaginary time calculations can overestimate or even underestimate the reaction rate. These behaviors are summarized in Figure 7.

4.5 Biological electron transfer

In recent years path integral methods have provided novel tools for investigating long-range electron transfer events in protein environments. One of the fundamental problems with regard to such processes concerns the magnitude of the donor-acceptor coupling matrix elements responsible for transfer and its relation to the intervening protein composition. While quantitative estimates of electronic coupling elements require complex and often prohibitively expensive electronic structure calculations, imaginary time path integral simulations have been extremely helpful in identifying electronic paths with significant contribution to the tunneling matrix element and revealing their spatial distribution.⁵⁴ Figure 8 shows four typical electron tunneling paths selected from a MCPI analysis applied to a ruthenium-modified myoglobin. These paths are seen to be largely confined within a tunneling tube that connects directly the donor to the acceptor. The thickness of the tube, i.e. the magnitude of the quantum fluctuations about the straight line path, is determined by the overall tunneling probability which in turn depends on the size of the tunneling barrier. A similar analysis can be carried out in terms of hole paths which offer a more appropriate description of such processes.⁵⁵

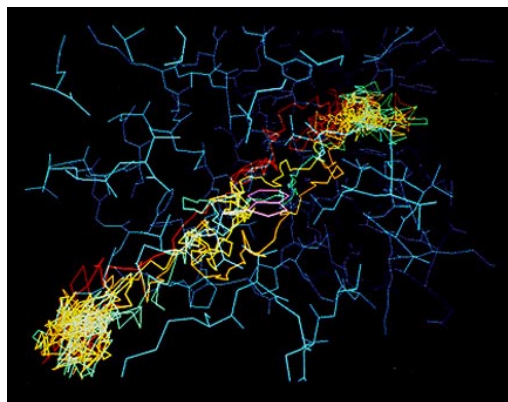


Fig. 8. Four quantum paths (depicted in red, yellow, orange and green) for the tunneling electron in ruthenium-modified myoglobin sampled from 5×10^5 paths of a Monte Carlo run. The protein is in light blue. The heme and ruthenium redox centers are separated by 28.2 Å center-to-center. Adapted from Ref. 54.

The dynamics of electron transfer processes in the condensed phase are ideally suited to real-time path integral calculations with the iterative methodology discussed in the previous section. Recently long-time simulations of the early stages of charge separation in bacterial photosynthetic reaction centers^{56,57} were reported⁵⁸ using the FPF methodology. These simulations employed a simple model of three electronic states which correspond to the photoexcited special chlorophyll pair (the donor), the reduced accessory chlorophyll (bridge) and the reduced bacteriopheophytin (the acceptor on the ten-to-hundred picosecond time scale). The coupling to the protein and water environment was included as a harmonic bath whose spectral density was obtained by inverting available classical trajectory data. There has been considerable debate concerning the values of the interstate couplings and the free energy of the accessory chlorophyll; for these reasons, these parameters were varied in the simulations until semi-quantitative agreement with experimental observations was reached. Through this procedure the reduced accessory chlorophyll state was estimated to have a free energy about 400 cm^{-1} lower than that of the electron donor. The corresponding mechanism involves to a good approximation two first-order kinetic steps, the second of which is fast compared to the first, leading to rapid depletion of transient bridge population.

5 CONCLUDING REMARKS

The path integral offers an insightful approach to time-dependent quantum mechanics and quantum statistical mechanics. In recent years a host of powerful numerical path integral methods have been developed which have enabled simulations of quantum many-particle systems not treatable by other means.

In spite of this progress several obstacles remain. Among the most important is the inability of current methodology to deal with the sign problem that arises in simulations of many-fermion systems and in real-time calculations with general many-body Hamiltonians. These issues remain at the forefront of computational quantum mechanics. Although the most general sign problem may not be solvable, there is probably significant room for progress in these directions which may enable accurate path integral simulations to address new, intriguing questions in chemistry and physics.

6 ACKNOWLEDGMENTS

This work has been supported by the David and Lucile Packard Foundation through a Packard Fellowship for Science and Engineering.

7 REFERENCES

1. Feynman R.P. *Rev. Mod. Phys.* 1948, 20, 367-387.
2. Feynman R.P.; Hibbs A.R. *Quantum Mechanics and Path Integrals*; McGraw-Hill: New York, 1965.
3. Doll J.D.; Freeman D.L.; Beck T.L. *Adv. Chem. Phys.* 1990, 78, 61.
4. Feynman R.P. *Statistical Mechanics*; Addison-Wesley: Redwood City, 1972.
5. Chandler D.; Wolynes P.G. *J. Chem. Phys.* 1981, 74, 4078-4095.
6. Feynman R.P.; F. L. Vernon J. *Ann. Phys.* 1963, 24, 118-173.
7. Leggett A.J.; Chakravarty S.; Dorsey A.T.; Fisher M.P.A.; Garg A.; Zwerger M. *Rev. Mod. Phys.* 1987, 59, 1-85.
8. Weiss U. *Quantum Dissipative Systems*; World Scientific: Singapore, 1993.
9. Metropolis N.; Rosenbluth A.W.; Rosenbluth M.N.; Teller H.; Teller E. *J. Chem. Phys.* 1953, 21, 1087.
10. Berne B.J.; Thirumalai D. *Annu. Rev. Phys. Chem.* 1986, 37, 401-424.
11. *Quantum Monte Carlo methods in condensed matter physics*, Suzuki M., Ed.; World Scientific: Singapore, 1993.
12. Thirumalai D.; Berne B.J. *Comp. Phys. Commun.* 1991, 63, 415-426.
13. Makri N. *Comp. Phys. Comm.* 1991, 63, 389-414.
14. Makri N. *J. Math. Phys.* 1995, 36, 2430-2456.
15. Makri N.; Miller W.H. *J. Chem. Phys.* 1988, 89, 2170-2177.
16. Doll J.D.; Freeman D.L. *Adv. Chem. Phys.* 1988, 73, 289-304.
17. Thirumalai D.; Berne B.J. *J. Chem. Phys.* 1984, 81, 2512-2513.
18. Behrman E.C.; Wolynes P.G. *J. Chem. Phys.* 1985, 83, 5863-5869.
19. Skilling J., in *Maximum entropy and Bayesian methods*, edited by J. Skilling (Kluwer Academic, Dordrecht, 1989).
20. Jarrell M.; Gubernatis J.E. *Phys. Rep.* 1996, 269, 133.
21. Galliccio E.; Berne B.J. *J. Chem. Phys.* 1994, 101, 9909-9918.
22. Galliccio E.; Berne B.J. *J. Chem. Phys.* 1996, 105, 7064-7078.
23. Onuchic J.N.; Wolynes P.G. *J. Phys. Chem.* 1988, 92, 6495-6503.
24. Marcus R.A. *Angew. Chem. Int. Ed. Engl.* 1993, 32, 1111-1121.
25. LeForestier C.; Bisseling R.; Cerjan C.; Feit M.D.; Friesner R.; Guldberg A.; Hammerich A.; Jolicard G.; Karlein W.; Meyer H.D.; Lipkin N.; Roncero O.; Kosloff R. *J. Comput. Phys.* 1991, 94, 59-80.
26. Kubo R.; Toda M.; Hashitsume N. *Statistical Physics*; 2nd ed; Springer-Verlag: Heidelberg, 1991.
27. Mak C.H.; Egger R. *Adv. Chem. Phys.* 1996, XCIII, 39-76.
28. Sim E.; Makri N. *Comp. Phys. Commun.* 1997, 99, 335-354.
29. Schnitker J.; Rossky P.J. *J. Chem. Phys.* 1987, 86, 3471-3485.
30. Parrinello M.; Rahman A. *J. Chem. Phys.* 1984, 80, 860-867.
31. Coker D.F.; Berne B.J.; Thirumalai D. *J. Chem. Phys.* 1987, 86, 5689.
32. Liu Z.; Berne B.J. *J. Chem. Phys.* 1993, 99, 9054-9069.
33. Landman U.; Scharf D.; Jortner J. *Phys. Rev. Lett.* 1985, 54, 1860-1863.

34. Barnett R.N.; Landman U.; Cleveland C.L.; Jortner J. *Phys. Rev. Lett.* 1987, 59, 811-814.
35. Lester Jr. W.A.; Hammond B.L. *Ann. Rev. Phys. Chem.* 1990, 41, 283-311.
36. Ceperley D.M.; Mitas L. *Adv. Chem. Phys.* 1996, 93, 1.
37. Ceperley D.M.; Jacucci G. *Phys. Rev. Lett.* 1987, 58, 1648-1651.
38. Marchi M.; Chandler D. *J. Chem. Phys.* 1991, 95, 889-894.
39. Chandler D. *J. Phys. Condens. Matter* 1990, 2, SA9-SA13.
40. *Activated barrier crossing*, Fleming G.R.; Hänggi P., Ed.; World Scientific: Singapore, 1993.
41. Miller W.H. *J. Chem. Phys.* 1974, 61, 1823-1834.
42. Tromp J.W.; Miller W.H. *J. Phys. Chem.* 1986, 90, 3482-3485.
43. Wolynes P.G. *J. Chem. Phys.* 1987, 87, 6559-6561.
44. Gillan M.J. *J. Phys. C* 1987, 20, 3621-3641.
45. Voth G.A.; Chandler D.; Miller W.H. *J. Chem. Phys.* 1989, 91, 7749-7760.
46. Zheng C.; McCammon J.A.; Wolynes P.G. *Proc. Natl. Acad. Sci. U.S.A.* 1989, 86, 6441-6444.
47. Kuharski R.A.; Bader J.S.; Chandler D.; Sprik M.; Klein M.L.; Impey R.W. *J. Chem. Phys.* 1988, 89, 3248-3257.
48. Gillan M.J. *Phys. Rev. Lett.* 1987, 58, 563-566.
49. Sun Y.-C.; Voth G.A. *J. Chem. Phys.* 1993, 98, 7451-7458.
50. Topaler M.; Makri N. *Chem. Phys. Lett.* 1993, 210, 285-293.
51. Miller W.H.; Schwartz S.D.; Tromp J.W. *J. Chem. Phys.* 1983, 79, 4889-4898.
52. Topaler M.; Makri N. *J. Chem. Phys.* 1994, 101, 7500-7519.
53. Hänggi P.; Talkner P.; Borcovec M. *Rev. Mod. Phys.* 1990, 62, 251-341.
54. Kuki A.; Wolynes P.G. *Science* 1987, 236, 1647-1652.
55. Onuchic J.N.; Beratan D.N.; Winkler J.R.; Gray H.B. *Ann. Rev. Biophys. Biom. Struc.* 1992, 21, 349.
56. Fleming G.R.; Grondelle R.V. *Physics Today* 1994, Feb. 1994, 49-55.
57. Deisenhofer J.; Norris J.R., Ed.; Academic Press: New York, 1993.
58. Sim E.; Makri N. *J. Phys. Chem.* 1997, 101, 5446-5458.

FIGURE CAPTIONS

1. A discretized path that connects the points (x_a, t_a) and (x_b, t_b) .
2. Schematic representation of a Feynman path in full-dimension system-bath space and its projection onto the reduced-dimension space characterized by the system coordinate alone. The gray curved lines indicate some of the nonlocal influence functional interactions arising from this projection.
3. Diagrammatic representation of the path integral interactions in a case where the memory length is equal to three time steps. The reduced density functionals that start at $t = 0$ and $t = 3\Delta t$ consist of paths specified by the time points shown as red and yellow circles, respectively. The coupling terms in the propagator connecting these two reduced density functionals are shown as cyan lines.
4. Electron path of a representative configuration in an octahedral unit simulation cell containing 300 water molecules (not drawn). The beads of the cyclic polymer are connected by straight lines. Adapted from Ref. 29.
5. Cluster configurations of $(\text{H}_2\text{O})_n^-$ via quantum path integral molecular dynamics simulations. Colored balls, large and small, correspond to oxygen and hydrogen, respectively. Colors of balls are chosen for visual perspective. The blue dots represent the electron (bead) distributions. Shown at the center is $(\text{H}_2\text{O})_8^-$ for a static molecular configuration. From top right and going counterclockwise: (i) diffuse surface state of $(\text{H}_2\text{O})_8^-$; (ii) surface state of $(\text{H}_2\text{O})_{12}^-$; (iii) surface state of $(\text{H}_2\text{O})_{18}^-$ (most stable structure); (iv) internal state of $(\text{H}_2\text{O})_{18}^-$. Adapted from Ref. 34.
6. A transition state from the simulated aqueous $\text{Fe}^{2+} - \text{Fe}^{3+}$ electron transfer. The two larger dark circles are the irons 5.5 \AA apart and the jagged lines connecting them is one path of the resonating electron. The Feynman paths of the quantized water molecules show the librations. Only a few of the hundreds of the simulated waters are depicted. Adapted from Ref. 39.
7. Quantum transmission coefficient for a symmetric double well potential interacting with a generic dissipative medium as a function of friction strength γ . The barrier height is denoted E_b and ω_b is the imaginary frequency at the top of the potential barrier. Solid squares: QUAPI results. Dashed line: results of centroid-density quantum transition state theory. (a) $E_b / k_b T = 10$ (activated regime with tunneling contributions). (b) $E_b / k_b T = 30$; for the first six data points (at small friction) the temperature is below crossover. Data from Ref. 52.
8. Four quantum paths (depicted in red, yellow, orange and green) for the tunneling electron in ruthenium-modified myoglobin sampled from 5×10^5 paths of a Monte Carlo run. The protein is in light blue. The heme and ruthenium redox centers are separated by 28.2 \AA center-to-center. Adapted from Ref. 54.